

Prevailing charge order in overdoped cuprates beyond the superconducting dome

Qizhi Li,^{1,*} Hsiao-Yu Huang,^{2,*} Tianshuang Ren,^{3,*} Eugen Weschke,⁴ Lele Ju,³ Changwei Zou,¹ Shilong Zhang,¹ Qingzheng Qiu,¹ Jiarui Liu,⁵ Shuhan Ding,⁵ Amol Singh,² Oleksandr Prokhnenko,⁴ Di-Jing Huang,² Ilya Esterlis,⁶ Yao Wang,⁵ Yanwu Xie,³ and Yingying Peng^{1,†}

¹*International Center for Quantum Materials, School of Physics, Peking University, Beijing 100871, China*

²*National Synchrotron Radiation Research Center, Hsinchu 30076, Taiwan*

³*Interdisciplinary Center for Quantum Information,*

State Key Laboratory of Modern Optical Instrumentation,

and Zhejiang Province Key Laboratory of Quantum Technology and Device,

Department of Physics, Zhejiang University, Hangzhou 310027, China

⁴*Helmholtz-Zentrum Berlin für Materialien und Energie, Berlin, Germany*

⁵*Department of Physics and Astronomy, Clemson University, Clemson, South Carolina 29631, USA*

⁶*Department of Physics, Harvard University, Cambridge, Massachusetts 02138, USA*

(Dated: October 19, 2022)

The extremely overdoped cuprates are generally considered to be Fermi liquid metals without exotic orders, whereas the underdoped cuprates harbor intertwined states. Contrary to this conventional wisdom, using Cu L_3 edge and O K edge resonant x-ray scattering, we reveal a charge order (CO) in overdoped $\text{La}_{2-x}\text{Sr}_x\text{CuO}_4$ ($0.35 \leq x \leq 0.6$) beyond the superconducting dome. This CO has a periodicity of ~ 6 lattice units with correlation lengths of $\sim 3 - 20$ lattice units. It shows similar in-plane momentum and polarization dependence and dispersive excitations as the CO of underdoped cuprates, but its maximum intensity differs along the c -direction and persists up to 300 K. This CO cannot be explained by either the Fermi surface instability or the doped Hubbard model and its origin remains to be understood. Our results suggest that CO is prevailing in the overdoped metallic regime and superconductivity emerges out of the CO phase upon decreasing hole carriers.

High-temperature superconductivity (SC) is a great surprise in quantum materials and its mechanism remains a puzzle. In the past 36 years, studies on cuprate superconductors primarily have been focused on the underdoped and optimally doped regions — close to the Mott-insulating state of the phase diagram [1, 2]. It has been a longstanding challenge to understand how the versatile phenomena exhibited in these materials, such as the pseudogap (PG) and strange metal states, together with a plethora of exotic electronic orders, coexist and compete with superconductivity [2]. On the contrary, the overdoped region is generally considered to be a conventional Fermi liquid (FL) and less affected by the doped-Mott-insulator scenario [1]. However, the doping and temperature dependencies of the superfluid density are incompatible with the standard BCS description, suggesting phase fluctuations in the overdoped region [3]. These fluctuations are characterized by photoemission as preformed Cooper pairs well above T_c [4] and magnetic fluctuations persistent in the extremely overdoped regime [5]. Moreover, ferromagnetism has been discovered in overdoped $(\text{Bi,Pb})_2\text{Sr}_2\text{CuO}_{6+\delta}$ (Bi2201) [6] and beyond the superconducting dome in $\text{La}_{2-x}\text{Sr}_x\text{CuO}_4$ [7]. These discoveries suggested that strong electronic correlations remain present in the overdoped cuprates.

Charge orders are ubiquitous in underdoped cuprates [2, 8–16] and has enigmatic interactions with SC [10, 11] and PG [12]; however, there is still no consensus on the underlying mechanism with on-going debates including the real-space electronic correlation scenario [14, 16] versus the momentum-space instability scenario [12]. The

latter has been challenged by one resonant X-ray scattering study that revealed charge order in heavily overdoped Bi2201 whose Fermi surface lacks the nesting features [17]. The CO provides a route by which to test how close the overdoped systems are to a FL, and also quantify the underlying fluctuations. Therefore, it is of great importance to assess the universality of charge ordering in overdoped cuprates, which will not only have the potential to elucidate the mechanism of CO instabilities but also provide a valuable perspective to understand the complex phase diagram coming from the overdoped regime.

In this Letter, we report the existence of charge order in heavily overdoped $\text{La}_{1.55}\text{Sr}_{0.45}\text{CuO}_4$ thin films beyond the superconducting dome (sample growth and characterizations are described in *Supplementary Sec.1*). The energy resolution of oxygen K -edge resonant inelastic x-ray scattering (RIXS) is ~ 30 meV at 41A Taiwan photon source. Figure 1(a) displays the schematic electronic structure of hole doped cuprates and illustrates the resonant absorption as well as the scattering processes at oxygen K -edge ($1s \rightarrow 2p$). The Zhang-Rice singlet (ZRS), originating from the hybridization between oxygen ligands and Cu $3d_{x^2-y^2}$ orbitals, manifests as a pre-edge peak in the x-ray absorption spectra (XAS) [18]. Figure 1(b) exemplifies the observed excitations in a metallic LSCO with $x = 0.45$ (resistivity shown in the inset of Fig. 1(b)), including the elastic peak, phonons (~ 0.05 eV), charge excitations (~ 0.6 eV) [20], and oxygen orbital excitations (> 1.5 eV). Given the relevance to CO [10, 21, 22], we focus on the elastic peak and low-energy

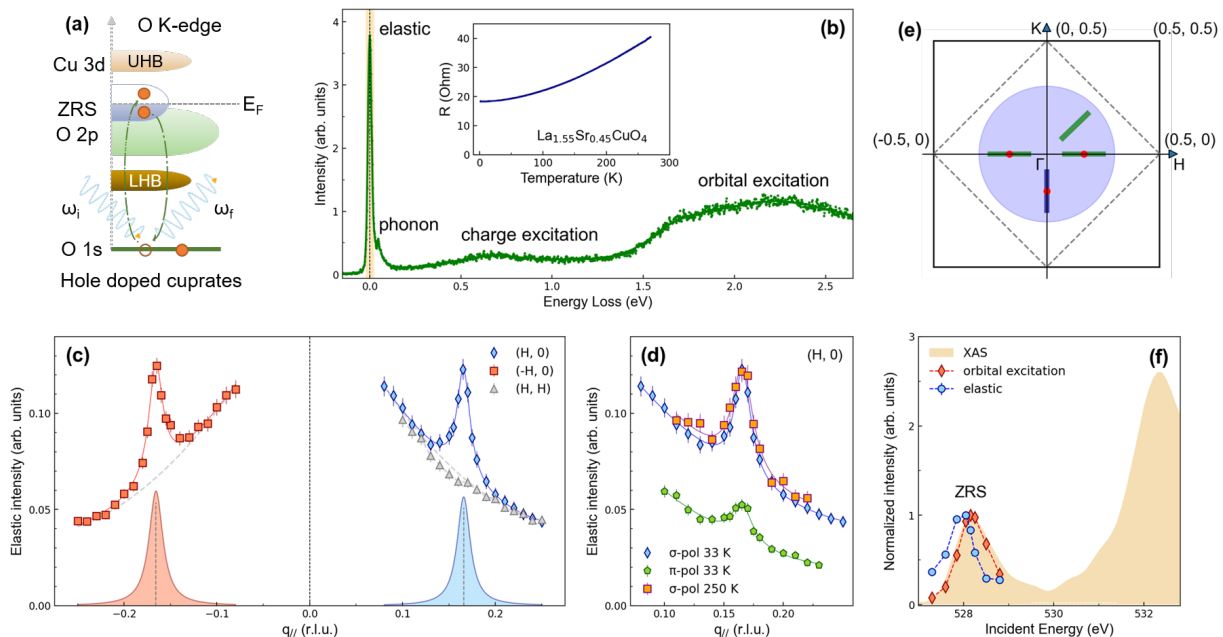


FIG. 1: Observation of charge order by RIXS in overdoped metallic $\text{La}_{2-x}\text{Sr}_x\text{CuO}_4$ ($x = 0.45$). (a) Schematic plot of RIXS process at O K -edge. (b) A typical RIXS spectrum at $\mathbf{q}_{||} = (0.12, 0)$, displaying the elastic peak, phonon, charge and orbital excitations. Inset: resistance curve displaying the metallic nature of the sample. (c) Integrated intensity of elastic peaks for positive and negative $(H, 0)$, and (H, H) directions, using σ polarization. Red and blue curves are Lorentzian peak fits to the data with a polynomial background (gray dashed lines). (d) Polarization measurements with σ - and π -polarized light, collected at 33 K and 250 K. (e) Reciprocal-space image. The Blue shaded region is the accessible momentum-transfer range of O K -edge. The green and blue lines indicate the momentum cuts, and red dots indicate the observed CO peaks. (f) XAS spectra near the Zhang-Rice Singlet (ZRS) absorption peak with σ -polarization at normal incidence. Incident energy dependence of the integrated intensity of elastic peak and orbital excitation, normalized to the value at the ZRS peak.

phonons below.

The elastic scattering displays a prominent peak at the planar wavevector $q_{||} = (0.165, 0)$. The full width at half-maximum (FWHM) of the peak is $\sim 0.017 \pm 0.002$ *r.l.u.* with a correlation length of ~ 70.8 Å. This feature is symmetric along both $(H, 0)$ and $(-H, 0)$ directions but absent along diagonal (H, H) directions (Fig. 1(c)) (see RIXS map in *Supplementary Fig. S5*). Its intensity is more pronounced for σ -polarization than for π -polarization (Fig. 1(d)), suggesting a predominant $d_{x^2-y^2}$ character of dopants forming the charge order. And this peak is nearly unchanged at temperatures as high as 250 K (Fig. 1(d)), which is similar to the CO in overdoped Bi2201 [17]. Moreover, this temperature-independent behavior is in line with the short-range high-temperature charge fluctuations (CDF) in the underdoped regions [24]. We also checked the resonant behaviour of this peak to reveal whether it originates from a modulation of the valence electrons. Figure 1(f) shows the intensity of the integrated elastic peak and orbital excitation as a function of incident photon energy compared with XAS. The orbital excitation follows the XAS spectrum, while the integrated elastic peak exhibits a clear resonance with a maximum slightly below the ZRS pre-peak. That is because XAS and scattering signals correspond to the imag-

inary and real parts of the atomic form factors, respectively. This trend is closely analogous to the behaviour of COs in underdoped cuprates [9, 22]. We have further excluded this peak as a trivial superstructure from hard x-ray scattering measurements (see *Supplementary Fig. S4*). Thus, we will refer to this feature as a CO peak below. Notably, here the CO wavevector $q_{\text{CO}} = (0.165, 0)$ is much smaller than that at underdoped LSCO samples — typically $q_{\text{CO}} \sim (0.23, 0)$ [16, 25, 26]. It nevertheless is close to the value in overdoped Bi2201 with $q_{\text{CO}} \sim (0.13, 0)$ [17], suggesting that charge instability with relatively long wavelength may prevail in heavily overdoped cuprates.

To investigate whether this CO signal originates from CuO_2 planes, we also perform Cu L -edge resonant energy integrated x-ray scattering (REIXS) measurements at Helmholtz-Zentrum Berlin. As shown in Fig. 2(a), we have measured the CO peak along $(0, -K)$ direction (blue cut in Fig. 1(e)) at both Cu L -edge and O K -edge and found it identical at the two edges, suggesting the strong hybridization between the Cu- $3d$ and the O- $2p$ orbitals. This result also demonstrates that the CO is bidirectional along H - and K -directions. Moreover, the CO peak measured by REIXS overlaps very well with the energy-integrated RIXS result (see *Supple-*

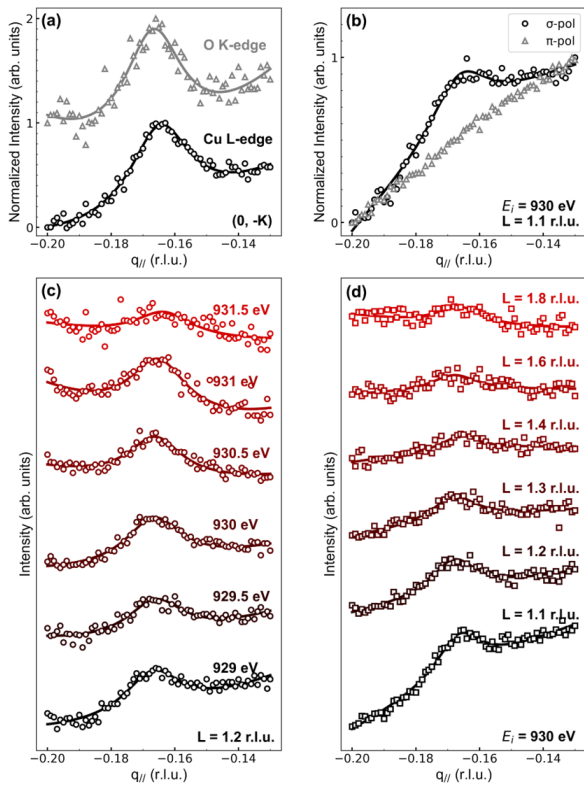


FIG. 2: Cu L_3 -edge and O K -edge REIXS studies of charge order in $\text{La}_{1.55}\text{Sr}_{0.45}\text{CuO}_4$. (a) Observation of charge order along $(0, -K)$ direction at both Cu L_3 -edge and O K -edge, offset is applied for clarity. (b) Polarization dependence of the charge order peak, collected at 930 eV and $L = 1.1$ r.l.u.. (c) Detuning measurements near the Cu L_3 -edge after self-absorption correction (see *Supplementary*). (d) L -dependence of charge order within the accessible range of $[1.1, 1.8]$ r.l.u. at 930 eV, collected with σ -polarization.

mentary Fig. S7), proving the consistency of the two experimental techniques. We again observe that the CO peak is stronger at σ -polarization than π -polarization at Cu L -edge (Fig. 2(b)) in favor of a charge origin [10]. Figure 2(c) shows the incident energy dependence of CO peak across Cu L_3 -edge, which does not display a clear resonant behavior due to a relatively poor energy resolution of ~ 1.3 eV of REIXS measurement. By selecting the incident x-ray energy at 930 eV with a prominent CO peak, we further investigate the L dependence of CO (Fig. 2(d)). We observe that the CO peak maximizes at $L = 1.1$ r.l.u. with smaller L value inaccessible, which is close to an integer L value. This is in sharp contrast to the behavior of CO in underdoped LSCO [26], which has a maximum at half-integer L due to the modulation of stripes along the c direction [27]. The different L behaviour may relate to the disappearance of spin glass behaviour beyond the critical doping of the pseudogap phase ($x_c \sim 0.19$) in LSCO [28], which is favoured by charge-stripe ordering. It is worth noting that CO in underdoped

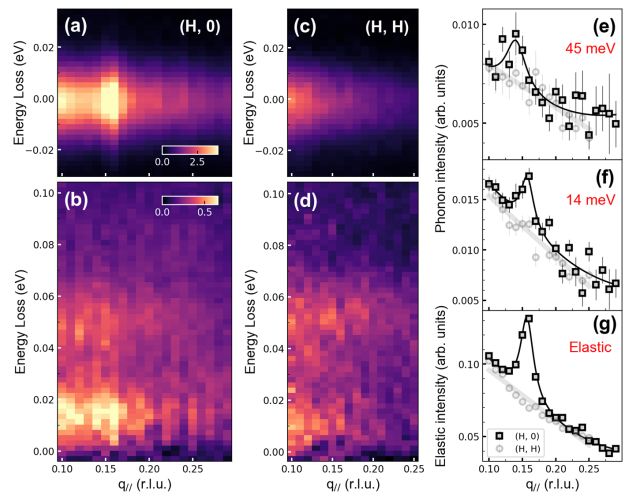


FIG. 3: Anisotropic momentum dependence of phonon intensity and dispersive CO excitations in $\text{La}_{2-x}\text{Sr}_x\text{CuO}_4$ ($x = 0.45$). (a, c) The elastic intensity map and (b, d) the inelastic RIXS intensity map for visualizing the CO and phonon branches along $(H, 0)$ direction and (H, H) direction, respectively. (e, f, g) Integrated intensity for buckling phonon, acoustic phonon and CO, respectively, along both directions. Details of the fitting are presented in *Supplementary Materials*.

$\text{YBa}_2\text{Cu}_3\text{O}_{6.67}$ can be enhanced by suppressing SC under magnetic field [29] or optical pump [30], which also shows a maximum at integer L values. The similar L -dependent behaviors of COs induced by the high magnetic field, optical pump and metallic regime suggest that they may have the same origin and be a common feature in the normal state.

To unveil the origin of CO it is crucial to investigate its collective excitations and the interplay between CO and phonons. In underdoped cuprates, it is widely observed that CO coexists with phonon intensity anomaly near the characteristic wavevector, accompanied by different magnitudes of phonon energy softening [16, 21–23, 25, 31]. These have been explained either by enhanced electron-phonon (e-ph) coupling [25] or interference between collective charge fluctuations and phonons [21, 22, 31]. Exploiting the high energy-resolution of O K -edge RIXS, we can probe CO and low-energy excitations at the same time. The RIXS map with better statistics and resolution (~ 25 meV) are visualized in Fig. 3(a). Notably, two phonon branches display pronounced enhancements of intensity near q_{CO} , while the phonon energy softening is negligible here. To quantify the q_{\parallel} dependence of the phonons, we fit the inelastic part of RIXS spectra and reveal three features at ~ 14 meV, ~ 45 meV and ~ 75 meV (See *Supplementary* Fig. S6). They can be assigned to the acoustic, bond-buckling and bond-stretching phonon modes, respectively, in accord with a recent RIXS study on the optimally doped LSCO [23]. Our intensity distribution curves show that

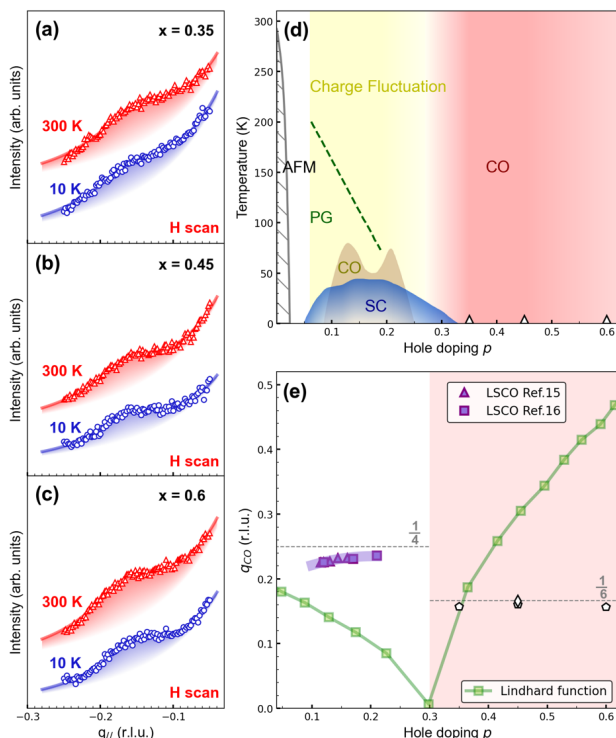


FIG. 4: Doping dependence of charge order in overdoped $\text{La}_{2-x}\text{Sr}_x\text{CuO}_4$ and the extended phase diagram. (a, b, c) CO peak profiles measured by Cu L -edge REIXS in LSCO with $x = 0.35, 0.45, 0.6$, respectively. The offset is applied for clarity. L is fixed at 1.1 r.l.u.. The peak is nearly temperature independent up to 300 K. (d) The extended CO phase diagram of cuprates. It shows superconducting dome defined by T_c , antiferromagnetism (AFM) defined by T_N [32], pseudogap (PG) determined from the Nernst coefficient [33], underdoped charge order and charge fluctuation [16, 24, 26] and overdoped charge order. (e) The doping dependence of the CO wave vector in LSCO and nesting vector obtained from Lindhard function.

acoustic (Fig. 3(e)) and buckling (Fig. 3(f)) branches are reinforced near q_{CO} (Fig. 3(g)), in concert with a proposed picture that dynamical CO excitations interfere with multiple phonon branches [21, 22, 31]. In stark contrast, no phonon intensity anomalies have been observed along (H, H) direction in the absence of CO (Fig. 3(c,d)), which suggests an intimate correlation between phonon and CO. We can further estimate the characteristic velocity of the dispersive CO excitations by connecting the maximal intensity anomaly of buckling mode at $q_A = 0.14$ r.l.u. with $q_{CO} = 0.16$ r.l.u., giving a velocity of $\sim 1.4 \pm 0.4$ eV \AA . This matches very well with the CO velocity of 1.3 ± 0.3 eV \AA in underdoped Bi2201 [22]. Our results indicate that dispersive CO excitations also exist in extremely overdoped regions, in analogy to those in underdoped regions.

To investigate the generality of this CO, we study the doping dependence of the CO on another batch of over-

doped LSCO thin films ($x = 0.35, 0.45, 0.6$) (Fig. 4). These films have a smaller thickness of 30 unit cells than the above-studied LSCO ($x = 0.45$) with 50 unit cells. We observe that the CO appears at $x = 0.35$ and gets more pronounced at $x = 0.45$ and 0.6 , which all persist from 10 K up to 300 K, as shown in Fig. 4, (a) to (c). We fit the REIXS spectrum with a Lorentz function for the peak and a Lorentz background from the specular tail, and the extracted peaks are shown in shaded areas. With smaller thickness, we observe that the CO peak displays a similar wavevector at ~ 0.166 r.l.u. but its correlation length becomes much shorter (~ 3 lattice units). This excludes the origin of CO driven from the substrate, while the thickness dependence remains to be understood. The observation of CO in extremely overdoped cuprates provides fresh insight for understanding the phase diagram (Fig. 4(d)). The presence of CO and AFM phases on the two sides of the superconducting dome is enlightening, suggesting that the unconventional superconductivity of cuprates can be regarded as an emergent phase out of either AFM or CO. This is consistent with the coexistence of short-ranged spin fluctuations and CO in the superconducting regime. Previous x-ray scattering studies report that the CO maximized at half-integer L values would disappear at $x \sim 0.25$ in LSCO [16, 26]. Here, the re-entrant CO exhibits distinct temperature and L dependencies, as well as different in-plane wave vectors, suggesting different interactions in play compared to CO in the underdoped region.

We then discuss the possible origins of this re-entrant overdoped CO. First, its emergence at the extremely overdoped region implies that it does not correlate with the pseudogap phase that ends at $x_c \sim 0.19$ [33]. We can also exclude the impact of the van Hove singularity, which was argued to cause the CDW phase in Bi2201 [17], since the Lifshitz transition occurs at much lower doping for LSCO ($x \sim 0.2$) [26]. Figure 4(e) shows the doping dependence of q_{CO} in LSCO [15, 16]. In the underdoped region, the CO wavevector increases with doping but close to 0.25 r.l.u. due to the proximity of spin and charge instabilities [34], while at the overdoped region it is likely to pin to a commensurate vector of $q_{CO} \sim 0.166$ r.l.u.. The Fermi-surface (FS) instabilities induced by the Coulomb interactions may lead to charge fluctuations in the sense of perturbation theory [35]. Accordingly, we have calculated the Lindhard function for LSCO and tracked the doping dependence of the FS nesting vector along the $(H, 0)$ direction. The nesting vector shows a non-monotonic behavior with a dip at $p \sim 0.3$ due to the Lifshitz transition from hole-like FS to electron-like FS (see *Supplementary Fig. S8*). This cannot account for the nearly doping-independent wavevector at $(0.166, 0)$, suggesting that the FS instability is an unlikely route to explain the CO in the overdoped regime.

We then consider nonperturbatively strong correlations of electrons, which have been found to persist in the

extremely overdoped cuprates [5]. With strong correlations, charge fluctuations are frozen at the Mott insulating phase and become negligible when the valence band is close to empty. Therefore, a dome-like structure is naturally expected in the strongly correlated Hubbard model upon doping (see *Supplementary Fig. S10*). However, the nature of the particle-hole excitations in the Hubbard model causes the leading instability at (0.5, 0.5), inconsistent with the observed charge mode. To explain the observed wavevector, we argue that it may be pinned by additional, longer-range interactions, which can be either remnant Coulomb repulsion or attraction mediated by bosonic modes, such as phonons [36]. In small-cluster simulations, we indeed observe the rise of a $q = (0.25, 0)$ [the smallest momentum accessible in the cluster] charge mode near 50% doping (see *Supplementary Fig. S11*). The dominance of this mode over the (0.5, 0.5) instability of the Hubbard model requires both relatively strong on-site and near-neighbor e-ph coupling besides the local Hubbard interaction. If the strong e-ph coupling is necessary for the experimentally observed CO, the absence of softening of phonons in our RIXS measurements suggests that other phonon mode(s) might be relevant, such as very low energy phonons observed in underdoped $\text{YBa}_2\text{Cu}_3\text{O}_{6.6}$ [37] and $\text{La}_{2-x}\text{Ba}_x\text{CuO}_4$ [38], that should be looked for in the future.

We note that recent work has realized superconductivity in highly overdoped $\text{La}_{2-x}\text{Ca}_x\text{CuO}_4$ thin films with doping levels up to $x = 0.5$ [39]. This invites future experiments to reveal the relationship between SC and CO in the extremely overdoped regime. Moreover, our findings resemble the layered dichalcogenides Cu_xTiSe_2 [40] and infinite-layer nickelate [41], where SC appears in the vicinity of charge order phase. This implies unusual competition between superconductivity and charge order states in broad correlated electron systems and motivates future investigations on unconventional superconductors.

We thank M. Grill, E. Huang, H. Yao, J. Zhang, X. J. Zhou, Y. Li, F. Wang, N. L. Wang, J. Feng, Z. Y. Weng for enlightening discussions. Y. Peng acknowledges the financial support from the National Natural Science Foundation of China (Grant No. 11974029) and the Ministry of Science and Technology of China (Grant No. 2019YFA0308401). Y. Xie acknowledges the financial support from the National Natural Science Foundation of China (Grant No. 12074334). I. E. and Y. W. acknowledge support from the National Science Foundation (NSF) award DMR-2038011. The RIXS experimental data were collected at beamline 41A of the National Synchrotron Radiation Research Center (NSRRC) in Hsinchu 30076, Taiwan. The REIXS experimental data were collected at the UE46-PGM1 beamline of Bessy-II (Helmholtz-Zentrum Berlin, Germany).

* These authors contributed equally to this work.

† Electronic address: yingying.peng@pku.edu.cn

- [1] Lee, P. A., Nagaosa, N. & Wen, X.-G. Doping a Mott insulator: Physics of high-temperature superconductivity. *Rev. Mod. Phys.* **78**, 17–85 (2006).
- [2] Keimer, B., Kivelson, S. A., Norman, M. R., Uchida, S. & Zaanen, J. From quantum matter to high-temperature superconductivity in copper oxides. *Nature* **518**, 179–186 (2015).
- [3] Božović, I., He, X., Wu, J. & Bollinger, A. Dependence of the critical temperature in overdoped copper oxides on superfluid density. *Nature* **536**, 309–311 (2016).
- [4] He, Y. *et al.* Superconducting Fluctuations in Overdoped $\text{Bi}_2\text{Sr}_2\text{CaCu}_2\text{O}_{8+\delta}$. *Phys. Rev. X* **11**, 031068 (2021).
- [5] Dean, M. P. M. *et al.* Persistence of magnetic excitations in $\text{La}_{2-x}\text{Sr}_x\text{CuO}_4$ from the undoped insulator to the heavily overdoped non-superconducting metal. *Nat. Mater.* **12**, 1019–1023 (2013).
- [6] Kurashima, K. *et al.* Development of Ferromagnetic Fluctuations in Heavily Overdoped $(\text{Bi,Pb})_2\text{Sr}_2\text{CuO}_{6+\delta}$ Copper Oxides. *Physical Review Letters* **121**, 057002 (2018).
- [7] Sonier, J. *et al.* Direct search for a ferromagnetic phase in a heavily overdoped nonsuperconducting copper oxide. *Proceedings of the National Academy of Sciences* **107**, 17131–17134 (2010).
- [8] Tranquada, J., Sternlieb, B., Axe, J., Nakamura, Y. & Uchida, S. Evidence for stripe correlations of spins and holes in copper oxide superconductors. *Nature* **375**, 561–563 (1995).
- [9] Abbamonte, P. *et al.* Spatially modulated ‘mottness’ in $\text{La}_{2-x}\text{Ba}_x\text{CuO}_4$. *Nat. Phys.* **1**, 155–158 (2005).
- [10] Ghiringhelli, G. *et al.* Long-Range Incommensurate Charge Fluctuations in $(\text{Y,Nd})\text{Ba}_2\text{Cu}_3\text{O}_{6+x}$. *Science* **337**, 821–825 (2012).
- [11] Chang, J. *et al.* Direct observation of competition between superconductivity and charge density wave order in $\text{YBa}_2\text{Cu}_3\text{O}_{6.67}$. *Nature Physics* **8**, 871–876 (2012).
- [12] Comin, R. *et al.* Charge Order Driven by Fermi-Arc Instability in $\text{Bi}_2\text{Sr}_{2-x}\text{La}_x\text{CuO}_{6+\delta}$. *Science* **343**, 390–392 (2014).
- [13] Peng, Y. Y. *et al.* Direct observation of charge order in underdoped and optimally doped $\text{Bi}_2(\text{Sr,La})_2\text{CuO}_{6+\delta}$ by resonant inelastic x-ray scattering. *Phys. Rev. B* **94**, 184511 (2016).
- [14] Cai, P. *et al.* Visualizing the evolution from the Mott insulator to a charge-ordered insulator in lightly doped cuprates. *Nature Physics* **12**, 1047–1051 (2016).
- [15] Wen, J.-J. *et al.* Observation of two types of charge-density-wave orders in superconducting $\text{La}_{2-x}\text{Sr}_x\text{CuO}_4$. *Nature Communications* **10**, 3269 (2019).
- [16] Lin, J. Q. *et al.* Strongly Correlated Charge Density Wave in $\text{La}_{2-x}\text{Sr}_x\text{CuO}_4$ Evidenced by Doping-Dependent Phonon Anomaly. *Phys. Rev. Lett.* **124**, 207005 (2020).
- [17] Peng, Y. *et al.* Re-entrant charge order in overdoped $(\text{Bi,Pb})_{2.12}\text{Sr}_{1.88}\text{CuO}_{6+\delta}$ outside the pseudogap regime. *Nat. Mater.* **17**, 697–702 (2018).
- [18] Chen, C. T. *et al.* Electronic states in $\text{La}_{2-x}\text{Sr}_x\text{CuO}_{4+\delta}$ probed by soft-x-ray absorption. *Phys. Rev. Lett.* **66**, 104–107 (1991).

- [19] Ament, L. J. P., van Veenendaal, M., Devereaux, T. P., Hill, J. P. & van den Brink, J. Resonant Inelastic X-ray Scattering Studies of Elementary Excitations. *Rev. Mod. Phys.* **83**, 705–767 (2011).
- [20] Nag, A. *et al.* Detection of Acoustic Plasmons in Hole-Doped Lanthanum and Bismuth Cuprate Superconductors Using Resonant Inelastic X-Ray Scattering. *Phys. Rev. Lett.* **125**, 257002 (2020).
- [21] Chaix, L. *et al.* Dispersive charge density wave excitations in $\text{Bi}_2\text{Sr}_2\text{CaCu}_2\text{O}_{8+\delta}$. *Nat. Phys.* **13**, 952–956 (2017).
- [22] Li, J. *et al.* Multiorbital charge-density wave excitations and concomitant phonon anomalies in $\text{Bi}_2\text{Sr}_2\text{LaCuO}_{6+\delta}$. *Proceedings of the National Academy of Sciences* **117**, 16219–16225 (2020).
- [23] Huang, H. Y. *et al.* Quantum Fluctuations of Charge Order Induce Phonon Softening in a Superconducting Cuprate. *Phys. Rev. X* **11**, 041038 (2021).
- [24] Arpaia, R. *et al.* Dynamical charge density fluctuations pervading the phase diagram of a Cu-based high T_c superconductor. *Science* **365**, 906–910 (2019).
- [25] Peng, Y. Y. *et al.* Enhanced Electron-Phonon Coupling for Charge-Density-Wave Formation in $\text{La}_{1.8-x}\text{Eu}_{0.2}\text{Sr}_x\text{CuO}_{4+\delta}$. *Phys. Rev. Lett.* **125**, 097002 (2020).
- [26] Miao, H. *et al.* Charge density waves in cuprate superconductors beyond the critical doping. *npj Quantum Mater.* **6**, 31 (2021).
- [27] Kimura, H. *et al.* Synchrotron x-ray diffraction study of a charge stripe order in $\frac{1}{8}$ -doped $\text{La}_{1.875}\text{Ba}_{0.125-x}\text{Sr}_x\text{CuO}_4$. *Phys. Rev. B* **67**, 140503 (2003).
- [28] Frachet, M. *et al.* Hidden magnetism at the pseudogap critical point of a cuprate superconductor. *Nature Physics* **16**, 1064–1068 (2020).
- [29] Gerber, S. *et al.* Three-dimensional charge density wave order in $\text{YBa}_2\text{Cu}_3\text{O}_{6.67}$ at high magnetic fields. *Science* **350**, 949–952 (2015).
- [30] Jang, H. *et al.* Characterization of photoinduced normal state through charge density wave in superconducting $\text{YBa}_2\text{Cu}_3\text{O}_{6.67}$. *Science Advances* **8**, eabk0832 (2022).
- [31] Lee, W. S. *et al.* Spectroscopic fingerprint of charge order melting driven by quantum fluctuations in a cuprate. *Nat. Phys.* **17**, 53–57 (2021).
- [32] Yamada, K. *et al.* Doping dependence of the spatially modulated dynamical spin correlations and the superconducting-transition temperature in $\text{La}_{2-x}\text{Sr}_x\text{CuO}_4$. *Phys. Rev. B* **57**, 6165–6172 (1998).
- [33] Wang, Y., Li, L. & Ong, N. P. Nernst effect in high- T_c superconductors. *Phys. Rev. B* **73**, 024510 (2006).
- [34] Nie, L., Maharaj, A. V., Fradkin, E. & Kivelson, S. A. Vestigial nematicity from spin and/or charge order in the cuprates. *Phys. Rev. B* **96**, 085142 (2017).
- [35] Dalla Torre, E. G., Benjamin, D., He, Y., Dentelski, D. & Demler, E. Friedel oscillations as a probe of fermionic quasiparticles. *Physical Review B* **93**, 205117 (2016).
- [36] Chen, Z. *et al.* Anomalously Strong Near-Neighbor Attraction in Doped 1D Cuprate Chains. *Science* **373**, 1235 (2021).
- [37] Le Tacon, M. *et al.* Inelastic X-ray scattering in $\text{YBa}_2\text{Cu}_3\text{O}_{6.6}$ reveals giant phonon anomalies and elastic central peak due to charge-density-wave formation. *Nature Physics* **10**, 52–58 (2014).
- [38] Miao, H. *et al.* Incommensurate Phonon Anomaly and the Nature of Charge Density Waves in Cuprates. *Phys. Rev. X* **8**, 011008 (2018).
- [39] Kim, G. *et al.* Optical conductivity and superconductivity in highly overdoped $\text{La}_{2-x}\text{Ca}_x\text{CuO}_4$ thin films. *Proceedings of the National Academy of Sciences* **118** (2021).
- [40] Morosan, E. *et al.* Superconductivity in Cu_xTiSe_2 . *Nature Physics* **2**, 544–550 (2006).
- [41] Rossi, M. *et al.* A broken translational symmetry state in an infinite-layer nickelate. *Nature Physics* **18**, 869–873 (2022).